CONFERENCE PRE-PRINT

DYNAMICS OF TURBULENCE AND ZONAL FLOWS EFFECTED BY TUNGSTEN IMPUITTY IN HL-2A EDGE PLASMAS

Q. Zou

Institute of Fusion Science, School of Physical Science and Technology, Southwest Jiaotong University Chengdu, China

Southwestern Institute of Physics

Chengdu, China

Email: qianzou@my.swjtu.edu.cn

J. Cheng

Institute of Fusion Science, School of Physical Science and Technology, Southwest Jiaotong University Chengdu, China

Z.B. Shi

Southwestern Institute of Physics

Chengdu, China

Y. Xu

Institute of Fusion Science, School of Physical Science and Technology, Southwest Jiaotong University Chengdu, China

L.W. Yan

Southwestern Institute of Physics

Chengdu, China

X. Chen

Institute of Fusion Science, School of Physical Science and Technology, Southwest Jiaotong University Chengdu, China

J. Chen

Institute of Fusion Science, School of Physical Science and Technology, Southwest Jiaotong University Chengdu, China

J.M. Gao

Southwestern Institute of Physics

Chengdu, China

Z.H. Huang

Southwestern Institute of Physics

Chengdu, China

N. Wu

Southwestern Institute of Physics

Chengdu, China

C.F. Dong

Key Laboratory of High-Performance Scientific Computation, School of science, Xihua University

Chengdu, China

W.C. Wang

Southwestern Institute of Physics

Chengdu, China

R.X. Huang

Institute of Fusion Science, School of Physical Science and Technology, Southwest Jiaotong University Chengdu, China

Z.S. Shi

Institute of Fusion Science, School of Physical Science and Technology, Southwest Jiaotong University Chengdu, China

X.O. Ji

Southwestern Institute of Physics

Chengdu, China

W.L. Zhong

Southwestern Institute of Physics

Chengdu, China

Abstract

The impact of tungsten impurity on the dynamics of turbulence and geodesic acoustic mode (GAM) zonal flows has been studied in HL-2A NBI-heated deuterium plasmas in detail. Experimental results show that the edge turbulence gradually

reduces after tungsten impurity injection, which is related to the increased electron-ion collisionality due to impurity stabilization mechanism. Meanwhile both the $E \times B$ mean and zonal flows decrease, which results from the increasing tungsten impurity concentration. The impurity-induced radiation belt remarkably shifts from edge toward core plasma, the edge local tungsten impurity concentration has a corresponding reduction, which is a main cause for the change in $E \times B$ mean flow. An important observation here is that the $E \times B$ mean flow start to rise as edge turbulence reduces to a rather low level, concurrently, the GAM zonal flows increase as well, which might result from the turbulent eddy symmetry-breaking by the $E \times B$ mean flow. The enhanced $E \times B$ mean and zonal flows are responsible for the consecutive stabilization of edge turbulence. The experimental results reveal the significant contribution from the local impurity concentration to the dynamic interplay between turbulence, $E \times B$ mean and zonal flow, which could advance the inherent physical mechanism governing turbulence and zonal flows in the presence of tungsten impurity in magnetized confined plasmas.

1. INTRODUCTION

With the transition from carbon-dominated first wall configurations to all-metal plasma-facing components (PFCs) in the design of international thermonuclear experimental reactor (ITER), the combination of impurity seeding and metal PFCs will bring up the problem of high-Z impurity sputtering [1]. Recently, tungsten (W) has been selected as the dominated PFCs material in the divertor region of ITER, due to its high heat tolerance, low erosion rate and low hydrogen retention [2, 3]. In general, the level of tungsten impurity concentration in a fusion reactor is roughly steady, but a transient increase of intrinsic tungsten impurity might occur in the case of burst events, i.e., edge-localized mode eruptions [4] and strong instability driven by high energy particle [5], which plays a critical role in plasma performance. It has been widely considered that the several instabilities existed in the plasmas always caused particle or energy loss and lead to confinement degradation. The one of the most important instabilities is the turbulence, which contributed the dominated abnormal transport [6]. Therefore, the study of effect played by high-Z tungsten impurity on turbulence and the resulting transport has attracted enormous interest in magnetically confined plasmas. The iron metal impurity has been observed to promote the edge-localized mode suppression via enhancing the turbulence at pedestal top and remain the high confinement state in HL-2A tokamak [7]. And the improved energy confinement with high-Z argon seeding at high density has also been reported in JT-60U device [8]. Recently, there are several explanations for the physical mechanism on how the impurity affect the turbulence and turbulent transport. Several theoretical works indicate that tungsten impurity has a stabilizing effect on trapped electron mode (TEM) or ion temperature gradient (ITG) turbulence when the impurity ion density profile is inwardly peaked [9, 10]. Meanwhile, the plasma dilution has also been thought responsible for the turbulence behavior effected by impurity ions, which is always correlated to the plasma parameter effective charge number (Z_{eff}) . The theoretical work in W7-X stellarator indicated that the impurity can significantly enhance or reduce turbulent ion loss dependent on the effective charge number [11]. And the possible contribution of Z_{eff} on global turbulence suppression has been put forward in LHD experimental results [12]. Another candidate is the flow shear, including mean and zonal flows [13, 14], could be affected by the impurity concentration, and then have a significant impact on the turbulence and transport. Such as the suppression of turbulence and transport reduction induced by the enhancement of E × B shearing rate in DIII-D tokamak [15, 16]. And in particular, a reduced turbulence regime accompanied by enhanced zonal flows due to the injected tungsten impurity was observed in HL-2A tokamak [17]. However, the underlying physical mechanism governing the turbulence activity involved the dynamical interplay between turbulence, mean and zonal flows in the presence of tungsten impurities still remains unclear.

2. EXPERIMENTAL SET-UP

The experimental results presented in this paper are from the NBI-heated deuterium plasmas on HL-2A tokamak (R = 1.65 m, a ≈ 0.4 m) with the limiter configuration under the following discharge parameters: $I_p \approx 150$ kA, $B_t \approx 1.36$ T, $n_{el} \approx (1.2-1.5) \times 10^{19}~m^{-3}$, $P_{NBI} \approx 100$ kW. The tungsten impurity was injected by the laser blow-off (LBO) system located at the outer mid-pane and the total number of injected tungsten particles could be roughly estimated to be about $(1-1.2) \times 10^{18}$ in the this experiment with the thickness (~5 µm), density of the tungsten layer (~19.35 g/cm³) and the size of the laser spot (~1 mm) on the target [18]. The main diagnostic used for the characteristics analysis of the turbulence, mean and zonal flows was a double-step Langmuir probe array [19]. Plotted in Fig. 1(a) are the magnetohydrodynamic equilibrium configuration reconstructed by the equilibrium fitting code (EFIT) together with the measurement location of the Langmuir probe. The probe has been installed at a reciprocating system at the mid-plane with a scanned speed of 1.0 m/s. The deepest distance of the reciprocating probe away from the last closed flux surface (LCFS) is almost at $\Delta r = -25$ mm, where the negative values of Δr mean inside the LCFS. Fig. 1(b) give the sketch of the double-step probe utilized in this work. Both the combination tips on each step are the standard four-tips probe, which could support for the measurement of the mean and fluctuating values of the floating potentials (V_f), ion saturated current (I_s), the local electron density (n_e), and temperature (T_e) according to the triple probe principle [20]. And the local radial particle

flux (Γ_r) could be calculated as $\Gamma_r = \langle n_e v_r \rangle$, where the radial velocity $v_r = E_p \times B_t$, and poloidal electric field could be calculated with two floating potential signals at different poloidal position. And similarly, the radial electric field E_r could be calculated with two floating potential signals at different radial position. The more detailed introduction about this doublestep reciprocating probe have been given in previous work [17] and let's simplify it here. It should be noted that the floating potential

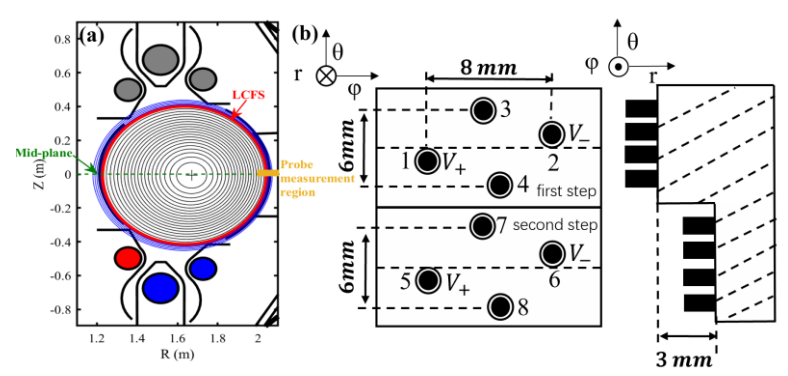


Fig. 1. The magnetohydrodynamic equilibrium configuration reconstructed by EFIT code and the location of the reciprocating Langmuir probe (a) and the sketch of this double-step Langmuir probe (b)

has always been considered as an alternative of the plasma potential in the Langmuir probe measurement, due to the much smaller level of the temperature fluctuation compared to potential fluctuation. And the tips here are carefully adjusted to minimize the phase error arising from the finite tip separation cross-field lines. The results presented here are well reproducible under similar discharge conditions.

3. EXPERIMENTAL RESULTS

3.1. Typical parameters evolutions with tungsten injection

In this work, we extend the analysis of earlier work [17] and address the inherent physical mechanism responsible for the lower turbulent level maintenance after the tungsten impurity injection in HL-2A edge plasmas. As presented in Fig. 2, the tungsten injection experiment could be divided into three time periods, i.e., before (t < 900 ms), during (900 < t < 940 ms) and after (t > 940 ms) impurity injection. One can see that the tungsten

impurity was injected at $t = 900 \, ms$, which could be confirmed by the significant increase in the spatiotemporal profile of the radiation power measured by the bolometer arrays [21], and the obvious rise both in effective charge number measured by visible bremsstrahlung diagnostics [22] and radiation intensity measured by space-resolved extreme ultraviolet (EUV) diagnostic [23] in Fig. 2(c) further indicates the tungsten impurity has been injected into the plasmas. An important observation is that the injected impurities are initially concentrated in the edge plasmas $(900 < t < 920 \, ms)$ and gradually transported into core plasmas $(t > 920 \, ms)$, as shown in Fig. 2(b). In our previous works, "after impurity injection (t > 940 ms)" is termed as a new state of reduced-turbulent transport, which is attributed to the enhancement of the GAM zonal flows effected by the injected tungsten impurity ions. And the period "during impurity injection (900 < t <940 ms)" has been considered as the 'transition phase', where both the Ha emission (not presented here) and edge electron temperature first significantly drop and then increased, whereas the plasma current (I_n) , lineaveraged density (n_{el}) and the plasma edge density (n_{e}) measured by probe located at $\Delta r = -25 \ mm$ exhibits a less pronounced change after tungsten injection, as shown in Fig. 2(a) and (d). For the characteristic analysis of the edge turbulent transport, the time-frequency spectrum of the radial particle flux has been calculated and plotted in Fig. 2(e). It could be seen that the particle loss mainly concentrated at $f = 20 - 60 \, kHz$, which is

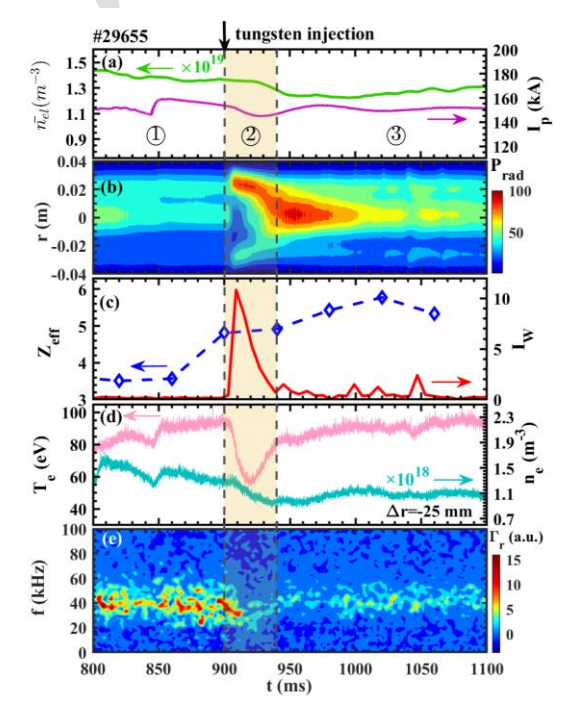


Fig. 2. Time evolutions of the line averaged density together with the plasma current (a), the radial distribution of the radiation power measured by the bolometer (b), the radiation intensity of W^{6+} and the effective charge number (c), the electron temperature and density (d) and radial particle flux (e) measured by the probe located at $\Delta r = -25$ mm.

roughly consistent with the turbulence frequency regime resolved on the density fluctuation spectrum. More importantly, on can see that the flux starts to drop immediately after the tungsten impurity injection, and then it keeps at a low fluctuation level starting from t = 920 ms. It seems that the time scale of turbulent transport reduction is comparable with the staying time of radiation belt localized in edge region. A question is naturally raised, what is the inherent physical mechanism responsible for sustaining the low turbulence level from t=920 ms? Actually, the enhanced zonal flow was considered responsible for the maintenance of the lower-level turbulence in the time period named "after impurity injection" in previous work [13], but the trigger for the amplification of zonal flows and the dynamical interaction between turbulence, mean and zonal flows in the time range of 900-940 ms has not been illustrated yet.

3.2 Turbulence and turbulence-driven flows dynamics during impurity injection

For further studying the dynamics of the turbulence and turbulence-driven flows effected by tungsten impurity, the behaviours of mean and GAM zonal flows during 900 ms < t < 940 ms has been analysed. Plotted in Figs. 3(a)-(b) are the time evolutions of the floating potential fluctuation filter in the GAM frequency (9-15 kHz) and the auto-power spectrum of floating potential fluctuation measured by the probe located at $\Delta r = -25$ mm, respectively. The coherent mode with frequency f=11.7 kHz has been confirmed to be GAM zonal flows in previous work. One can see that the GAM zonal flow was first decreased at the moment of the tungsten impurity

injection, however the downtrend lasted only 20 ms and then the zonal flow intensity gradually recovered and even increased to a higher level than that before impurity injection, as shown by the yellow shaded area in Figs. 3(a)-(b). For a more intuitively analysis of its behavior during this period, we have divided this period into two phases: phase-I from 900 to 920 ms (blue shaded area) and phase-II from 920 to 940 ms (red shaded area), as shown in Figs. 3(c)-(e). Figs. 3(c)-(d) presented the time traces of the root mean square (RMS) of the GAM zonal flows component $(\tilde{V}_{f\,GAM}^{RMS})$ in the floating potential fluctuation and the derivative of the $\tilde{V}_{f\ GAM}^{RMS}$ in the time domain, respectively. It could be observed that the GAM zonal flows significantly reduced in phase I, companied by a continuous negative value in derivatives in this phase, as shown by the blue shaded area. However, both the $\tilde{V}_{f \; GAM}^{RMS}$ and its derivative start changing in reverse after t=920 ms and remain this reverse variation among the total period in phase II, as shown in red shaded area. As mentioned in the previous work, the increased $E \times B$ shear flow might play active role in stretching turbulence eddies, which leads to a higher energy transfer rate from turbulence to GAM zonal flows after impurity injection ($t > 940 \, ms$), compared to that before impurity injection ($t < 900 \, ms$). In order to further support the crucial role played by $E \times B$ mean shear flow in modulating the variation of GAM zonal flows, the $E \times B$ mean flow velocity $(V_{E \times B})$, replaced by the averaged poloidal phase velocity of turbulence in absence of the plasma potential measurement, has been calculated and plotted in Fig. 3(e). Here the estimated poloidal phase velocity $(\bar{v}_{\theta,ph})$ was formalized as

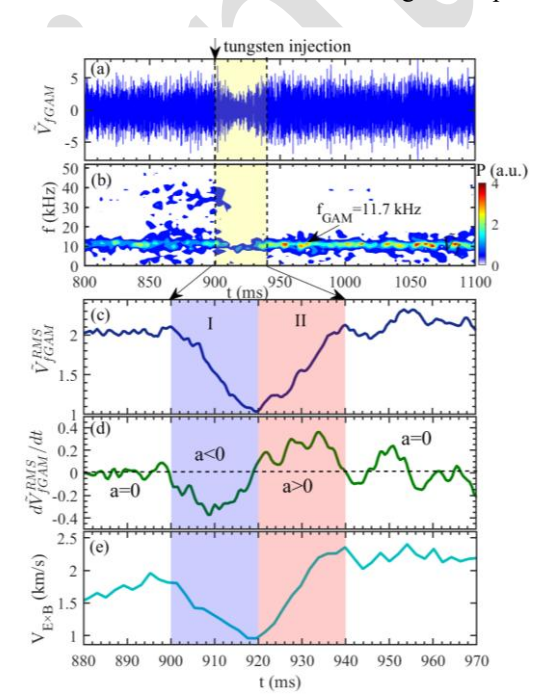


Fig. 3. The time traces of the floating potential fluctuation filter in GAM frequency (9-15 kHz) (a), the spectrogram estimated by the floating potential fluctuation (b), the zoomed-in plots: the GAM amplitude (c), the growth rate of GAM (d), and the $E \times B$ mean flow velocity, replaced by the averaged poloidal phase velocity ($\bar{v}_{\theta ph}$) in absence of the plasma potential measurement (e).

 $\bar{v}_{\theta,ph} = \sum_{k,f} S(k_{\theta},f) \cdot (2\pi f/k_{\theta}) / \sum_{k,f} S(k_{\theta},f)$, where the spectra width σ_k is computed by the statistical dispersion relation $(\sigma_k^2)^{1/2} = [\sum_f \sum_k [k - \bar{k}(f)]^2 \cdot s(k|f) \cdot s(f)]^{1/2}$ and the frequency is integrated in $f = 20 - 500 \, kHz$. The $\bar{v}_{\theta,ph}$ has always been used as a proxy of $E_r \times B$ mean flow $(V_{E\times B})$ in several experiments [24, 25] One can see that during the impurity injection, the $V_{E\times B}$ firstly went down in phase I, and then it increased in phase II. Fully indicated that the injected tungsten impurity could affect the GAM zonal flows via changing the $E\times B$ mean shear flow.

For further investigated the $E \times B$ mean flow variation during the tungsten impurity injection, the statistical data of the $E \times B$ mean flow velocity $(V_{E \times B})$ versus the impurity concentration (f_z) averaged in these two phases have been plotted in Fig. 4(a). The impurity concentration is roughly estimated as $f_z = n_z/n_e \approx \frac{I_w}{n_e^2 L_z(T_e)}$, where

 I_w is the radiation power of the W^{6+} line measured by an extreme ultraviolet spectrometer [26], n_e is the local plasma density and $L_z(T_e)$ represents the emission coefficient, which is almost constant against the electron temperature in the range of $60 \ eV < T_e < 100 \ eV$. $\Delta t = 0$ in the color-bar indicates the initial time of tungsten impurity injection. As expected, for a few milliseconds (~3ms) after the increased tungsten impurity concentration,

the $E \times B$ mean flow velocity kept almost un-changed, and gradually, the flow velocity is inversely proportional increased impurity concentration. The relation presented indicates the decisive impact of local tungsten impurity concentration on determining E × B mean flow. However, it could be observed the although the $E \times B$ mean flow was still slowing down when the impurity concentration began to decline, finally the enhanced $E \times B$ mean flow velocity occur at the appointed time with the cautiously decreasing impurity concentration. For the physical mechanism responsible for

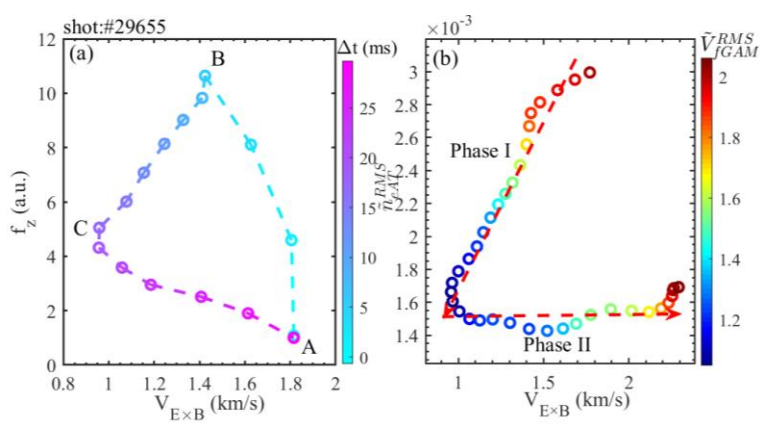


Fig. 4. The $E \times B$ mean flow velocity versus the impurity concentration in phase I and phase II. The relation among the turbulence, mean and zonal flows (b).

the influence of impurity ions on radial electric field (E_r) , there are several potential possibilities displayed follow: (i) ion-impurity collision might cause the momentum loss via the collision term related to $v_{iz} \propto Z^2 n_z/T_i^{3/2}$ (n_z means the impurity density, Z is the impurity charge number), and suppress poloidal rotation [27]; (ii) the main ion density would be diluted by the impurity ions, and the main ion pressure and the pressure gradient-driven radial electric field might reduce in term of the plasma quasi-neutrality condition ($n_e = n_i + Zn_z$) [28]; (iii) impurity might enhance energy loss through the radiation mechanism, leading to a decrease in plasma edge temperature [29], which in turn affects the radial electric field; (iv) impurities may alter the characteristics of drift wave turbulence, which could drive the poloidal rotation (radial electric field) via the momentum transport [30]. The relevant physical mechanisms mentioned above still need more experimental evidence in future works.

Mean and zonal flows are generally thought to be effective in suppressing turbulence via the shearing effect [31]. For elucidating the dynamics of turbulence, mean and zonal flows effected by tungsten impurity ions, the relationship among the turbulence, mean and zonal flows in the two phases has been given in Fig. 4(b). Here the RMS of the density fluctuations filter in ambient turbulence frequency region ($\tilde{n}_{e\,AT}^{RMS}$), i.e., 20-60 kHz has been utilized to represent turbulence level, and the $V_{E\times B}$ and $\tilde{V}_{f\,GAM}^{RMS}$ are on behalf of mean and GAM zonal flows, respectively. One can see that all of the turbulence and turbulence-driven flows (mean and zonal flows) are decreased in phase I. Thus it is important to elucidate the reason one by one why turbulence and two flows will decrease with impurity injection in this phase. Firstly, for the turbulence observed here, we have calculated the poloidal wave number (k_{θ}) by using two-point correlation analysis [32], which is roughly valued as $k_{\theta} \approx$ $1.5 \sim 2.1 \ cm^{-1}$. Considered the turbulence in this work propagated in the electron diamagnetic direction and was accompanied with a quasi-coherent mode (QCM) characteristic, it could be roughly judged as TEM turbulence [33]. The theoretical work [10] has indicated that the increased collisionality could weaken the trapped electron response and lead to a more stable TEM turbulence, which has also been confirmed in experimental works [34, 35]. In this work, the enhanced electron- ion collisionality has been observed in phase I, which further confirm the stabilized effect of tungsten impurity on edge turbulence via increased collisionality. Additionally, the $E \times B$ shearing effect, one widely-recognized effective factor to cause turbulence stabilization with impurity injection, has been excluded for the reduced $E \times B$ mean flow velocity in phase I. Moreover, for the reduced GAM zonal flows in this phase, the time trace of the summed biacoherence, which could be a rough estimation of the driving term provided from non-zonal turbulence to GAM zonal flows, has been observed reduced in this phase. And the collisional damping of zonal flows with considering the impurity effect was calculated and increased significantly in this phase. However, the effect of tungsten impurity on GAM zonal flows Landau damping has been excluded due to the nearly unchanged GAM frequency presented in the previous work [17]. Thus it could be concluded that the reduced E × B mean flow together with the increased collisional damping contributed to the reduced GAM zonal flows in phase I. As for the reason why impurity injection could cause the E × B mean flow reduction, the potential possibilities have been described in the earlier.

The surprising observation occurred in phase II, i.e., the turbulence has been controlled at a lower level, accompanied with gradually increased and finally higher flow level of mean and zonal component compared to

the period before impurity injection, as shown in Fig. 4(b). As we have proposed, the injected impurity ions cloud directly influence the edge turbulence with several known physical mechanism in phase I, considering the tungsten impurity was concentrated at the edge area in this phase, as shown in Fig. 2(b). However, it could be observed that the impurity concentration in edge plasma was rapidly decreased with more radiation power concentrated in core plasma, as shown in Figs. 2(b)-(c). Thus the stabilization effect of tungsten impurity on edge turbulence could be weaken due to the tungsten impurity behavior in phase II. As mentioned before, the important observation is that both the mean and GAM zonal flows were significantly enhanced and even exceed the initially value compared before impurity injection in this phase. The flows shearing effect, include mean and zonal, contributed a synergistic effect for stabilizing the edge turbulence via turbulent eddy symmetry-breaking process [36]. Meanwhile, the increased E × B mean flow and the decreased collisional damping rate together promote the enhanced GAM zonal flows. All the results concluded here indicates that the effect of tungsten impurity ions on the edge turbulence, mean and zonal flows dynamics could vary, even within a small timescale (~40 ms), which might be related to the radial distribution of the impurity radiation intensity. And this founding could offer a more precise physical mechanism of the effect of tungsten impurity on turbulence and zonal flows.

3.3 Turbulence spreading mitigation by impurity ions

It's well recognized that the turbulence spreading, i.e., turbulence penetration from the initially location into surrounding areas, could results in global confinement degradation while enhancing ion temperature profile stiffness [37]. How is turbulence spreading changed among the variation of turbulence dynamics (reduction and maintenance) during the impurity injection? In order to observe the changes in turbulence more intuitively and

meticulously, the initial turbulence fluctuation level estimated from the component of the electron density fluctuation filtered in turbulence frequency (20-100 kHz) has been plotted in Fig. 5(a). It could be seen clearly that the turbulence fluctuation level decreased quickly in phase I. recovered slightly in phase II and ultimately maintain at a lower level after impurity injection (t>940 ms), which is consistent with the observation in the time-frequency spectrogram of density fluctuation presented in Fig. 2(e). Plotted in Fig. 5(b) are the time traces of the shear rates of the E × B mean flow (γ_{mean}) and GAM zonal flows (γ_{GAM}) , which are roughly estimated as $\gamma_{mean} = \Delta V_f^{mean}/(\Delta r^2 B)$, $\gamma_{GAM} = k_r^2 \Delta V_f^{GAM}/B$, respectively, where ΔV_f^{mean} means the time-averaged floating potentials across the radial scale Δr , and ΔV_f^{GAM} represents the fluctuating level of the GAM zonal flows estimated by the RMS of floating potential fluctuation filtered in the GAM frequency (9-16 kHz) [38]. Here it should be noted that the effective shearing rate of GAM zonal flows roughly reduced about 10% compared to the measured shearing rate, with considering the ratio of GAM frequency ($f_{GAM} = 11.7 \, kHz$) to the turbulence spectral width ($\Delta \omega = 60 \, kHz$) [39]. One can see that the reduction of the shearing rate both occur in E × B mean and zonal flows in phase I, significantly proved that the edge tungsten impurity concentration replaced the mean and zonal flows shearing, leading to the stabilization of turbulence in this phase. As mentioned earlier, the reduced zonal flows in this phase are mainly attributed to the decreased $E \times B$ mean flow shear and partially to the increased collisional damping rate. When the tungsten gradually penetrated to the core region, the rising shearing rates of mean together with

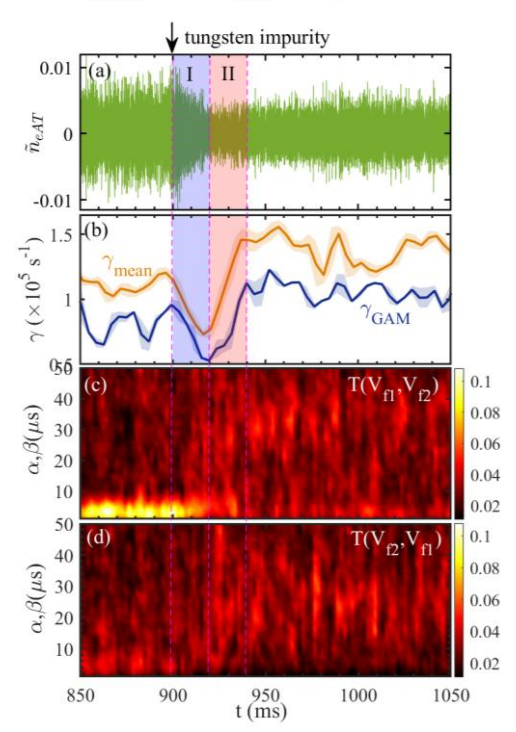


Fig. 5. The time evolutions of the turbulence fluctuation level (a), the shearing rates of mean and zonal flows (b), the transfer entropy between two radially displaced floating potential fluctuations (c-d), where V_{f1}/V_{f2} are located at inner/outer position, respectively.

zonal flows are responsible for the mitigation of turbulence in phase II and promote the long-time stabilization after impurity injection. The transfer entropy [40], a measurement of the causal relation or information between two time series, has been utilized here for the judgement of the direction and intensity of turbulence spreading. For example, a measure of information transfer between the two time series X and Y is given by:

$$T_{Y-X} = \sum p(x_{n+1}, x_{n-k}, y_{n-k}) \log_2 \frac{p(x_{n+1}|x_{n-k}, y_{n-k})}{p(x_{n+1}|x_{n-k})}$$
(1)

Where p(a|b) is the probability distribution of a conditional on b, p(a|b) = p(a,b)/p(b). If Y has no influence on the immediate future evolution of system X, one has $p(x_{n+1}|x_{n-k},y_{n-k}) = p(x_{n+1}|x_{n-k})$, so that $T_{Y-X} = 0$. Generally, T_{Y-X} could be compared with T_{X-Y} to uncover a net information flow [41]. Given in Figs. 5(c)-(d) are the comparison of the transfer entropy between two floating potential fluctuations measured from tow radially displaced probe pins. One can see that the transfer entropy detects a clear time delay ($\sim 3 \mu s$) from V_{f1} (inner position) to V_{f2} (outer position) in Fig. 5(c). However, the similar time delay not occurred in the case from V_{f2} to V_{f1} in Fig. 5(d), indicates a unidirectional energy transfer from V_{f1} to V_{f2} , which means the outwardly turbulence spreading. And the observations presented here indicates that the turbulence spreading has an obvious drop at the time of impurity injection, and almost disappear at the period after impurity injection. Thus it could be concluded that the turbulence spreading would be modulated by the turbulence and zonal flows dynamics with the tungsten impurity, which could be beneficial for the protection of the plasma first wall by mitigate the plasma-wall interaction.

4. SUMMARY

In summary, the experimental observation presented here studied the dynamics of turbulence and zonal flows effected by the tungsten impurity in HL-2A NBI-heated deuterium plasmas. Results show that the dynamics of turbulence and GAM zonal flows distinct in two phases due to the different concentrated location of tungsten impurity. In phase I, the edge turbulence characterized by TEM turbulence would be stabilized directly contributed to the injected massive tungsten impurity located at edge plasmas. And the reduced GAM zonal flows is the result of the decreased $E \times B$ mean flow shear effected by a rising impurity concentration and the enhanced collisional damping rate. The former could eliminate the driving energy transfer from turbulence to GAM zonal flows and the later could amplify the damping process of zonal flows. In phase II, the maintain of the lower turbulence depends on the enhanced $E \times B$ mean and zonal flows shear, and the $E \times B$ mean flow shear has also account for the amplified GAM zonal flows by promoting the elongation of turbulence eddies. Thes experimental results here reveal the dynamics of edge turbulence and zonal flows effected by tungsten impurity, which could provide an in-depth perspective on the inherent physical mechanism of the edge turbulence behavior with the tungsten impurity existence.

ACKNOWLEDGEMENTS

This work is partially supported by the National Science Foundation of China under grant Nos. 12175186, the Chinese National Fusion Project for ITER under Grant Nos. 2022YFE03070001, and the National Magnetic Confinement Fusion Science Program of China under Grant Nos. 2024YFE03190001.

REFERENCES

- [1] K. Krieger, S. Brezinsek, J.W. Coenen *et al* Scrape-off layer and divertor physics Chapter 5 of the special issue: on the path to tokamak burning plasma operation *Nucl. Fusion* 65 (2025) 043001
- [2] R.C. Isler Impurities in tokamaks Nucl. Fusion 24 (1984) 1599–1678
- [3] D. Naujoks, K. Asmussen, M. Bessenrodt-Weberpals *et al* Tungsten as target material in fusion devices *Nucl. Fusion* 36 (1996) 671
- [4] G.L. Xu, R. Ding, F. Ding et al An interpretive model for the double peaks of divertor tungsten erosion during type-I ELMs in EAST, Nucl. Fusion 61 (2021) 086011
- [5] B.I. Khripunov, A. Brukhanov, V. Gureev *et al* Plasma effect on tungsten damaged by high-energy alpha particles: Erosion and deuterium trapping *J. Nucl. Mater.* 415 (2011) S649-S652
- [6] P.W. Terry Suppression of turbulence and transport by sheared flow, Rev. Mod. Phys. 72 (2000) 109-65
- [7] Y.P. Zhang, D. Mazon, X.L. Zou *et al* 2018 Control of edge localized modes by pedestal deposited impurity in the HL-2A tokamak, *Nucl. Fusion* 58 (2018) 046018
- [8] H. Urano, M. Nakata, N. Aiba et al Roles of argon seeding in energy confinement and pedestal structure in JT-60U, Nucl. Fusion 55 (2015) 033010
- [9] J.Q. Dong and W. Horton Studies of impurity mode and ion temperature gradient mode in toroidal plasmas *Phys. Plasma* 2 (1995) 3412
- [10] H.R. Du, Z.X. Wang and J.Q. Dong Impurity effects on trapped electron mode in tokamak plasmas *Phys. Plasma* 23 (2016) 072106
- [11] J.M. Garcia-Regana, I. Calvo, F.I. Parra *et al* Reduction or Enhancement of Stellarator Turbulence by Impurities *Phys. Rev. Lett.* 133 (2024) 105101

- [12] F. Nespoli, S. Masuzaki, K. Tanaka *et al* Observation of a reduced-turbulence regime with boron powder injection in a stellarator *Nat. Phys.* 18 (2022) 350–6
- [13] K.H. Burrell Effects of E×B velocity shear and magnetic shear on turbulence and transport in magnetic confinement devices *Phys. Plasmas* 4 (1997)1499
- [14] G.D. Conway, A.I. Smolyakov, T. Ido *et al* Geodesic acoustic modes in magnetic confinement devices *Nucl. Fusion* 62 (2022) 013001
- [15] M. Murakami, G.R. McKee, G.L. Jackson *et al* Physics of confinement improvement of plasmas with impurity injection in DIII-D *Nucl. Fusion* 41 (2001) 317
- [16] G. Mckee, K. Burrell, R. Fonck et al Impurity-Induced Suppression of Core Turbulence and Transport in the DIII-D Tokamak, Phys. Rew. Lett. 84 (2000) 1922
- [17] Q. Zou, J. Cheng, Z.B. Shi *et al* Observation of reduced-turbulence regime with tungsten injection in HL-2A edge plasmas *Nucl. Fusion* 63 (2023) 126029
- [18] C.F. Dong, S. Morita, Z.Y. Cui *et al* Evaluation of tungsten influx rate and study of edge tungsten behavior based on the observation of EUV line emissions from W6+ ions in HL-2A Nucl. Fusion 59 (2019) 016020
- [19] L.W. Yan, W.Y. Hong, K.J. Zhao et al Novel design for zonal flow probe arrays in the HL-2A tokamak Rev. Sci. Instrum. 77 (2006) 113501
- [20] S.-L. Chen and T. Sekiguchi Instantaneous Direct-Display System of Plasma Parameters by Means of Triple Probe *J. Appl. Phys.* 36 (1965) 2363
- [21] J.M. Gao, Y. Liu, W. Li et al Minimum Fisher regularization of image reconstruction for infrared imaging bolometer on HL-2A Rev. Sci. Instrum. 84 (2013) 093503
- [22] L. Liu, D.L. Yu, W.J. Chen *et al* Zeff Measurement in Ohmic, L-andH-Mode Plasmas on HL-2A Tokamak IEEE Trans. *Plasma Sci.* 30 (2020) 10560
- [23] C.F. Dong, S. Morita, L. Feng *et al* Space-resolved extreme ultraviolet spectrometer for impurity diagnostics in HL-2A *Fusion Eng. Des.* 159 (2020) 111785
- [24] Y. Xu, M. Van Schoor, R.R. Weynants *et al* Edge turbulence during the static dynamic ergodic divertor experiments in TEXTOR *Nucl. Fusion* 47 (2007) 1696–1709
- [25] P. Manz, D Prisiazhniuk, T Happel *et al* On the phase velocity in between weak and strong plasma edge turbulence *Plasma Phys. Control. Fusion* 60 (2018) 085002
- [26] C.F. Dong, S. Morita, M. Gota et al Space-resolved extreme ultraviolet spectrometer for impurity emission profile measurement in Large Helical Device Rev. Sci. Instrum. 81(2010) 033107
- [27] C. Angioni Impurity transport in tokamak plasmas, theory, modelling and comparison with experiments *Plasma Phys. Control. Fusion* 63 (2021) 073001
- [28] R.R. Dominguez and G.M. Staebler Impurity effects on drift wave stability and impurity transport Nucl. Fusion 33 (1993)
- [29] R.V. Jensen, D.E. Post, W.H. Grasberger *et al* Calculations of impurity radiation and its effects on tokamak experiments *Nucl. Fusion* 17 (1977) 1187
- [30] S. Moradi, M. Z. Tokar and B. Weyssow Modeling of impurity effect on drift instabilities in plasmas with many ion species *Phys. Plasmas* 17 (2010) 012101
- [31] G.D. Conway, C. Angioni, F. Ryter *et al* Mean and Oscillating Plasma Flows and Turbulence Interactions across the L-H Confinement Transition *Phys. Rev. Lett.* 106 (2011) 065001
- [32] J.M. Beall, Y.C. Kim and E.J. Powers Estimation of wavenumber and frequency spectra using fixed probe pairs *J. Appl. Phys.* 53 (1982) 3933
- [33] H Arnichand, J Citrin, S Hacquin *et al* Identification of trapped electron modes in frequency fluctuation spectra *Plasma Phys. Control. Fusion* 58 (2016) 014037
- [34] G Bodner, C Bourdelle, P Manas et al Stability analysis of WEST L-mode discharges with improved confinement from boron powder injection *Plasma Phys. Control. Fusion* 66 (2024) 045022
- [35] M.Y. Wang, J. Li, Y.K. Bai et al Particle pump-out induced by trapped electron mode turbulence in electron cyclotron heated plasmas on XuanLong-50 spherical torus Nucl. Fusion 63 (2023) 076024
- [36] P. Manz, M. Ramisch, and U. Stroth Physical Mechanism behind Zonal-Flow Generation in Drift-Wave Turbulence Phys. Rev. Lett. 103 (2009) 165004
- [37] S. Yi, J.M. Kwon, P.H. Diamond *et al* Turbulence spreading as a non-local mechanism of global confinement degradation and ion temperature profile stiffness *Nucl. Fusion* 55 (2015) 092002
- [38] T. S. Hahm, M. A. Beer, Z. Lin et al Shearing rate of time-dependent E×B flow. Phys. Plasmas 6 (1999) 922-926
- [39] C. Silva, P Duarte, H Fernandes *et al* Interaction between mean and fluctuating E×B shear flows on the ISTTOK edge plasma *Plasma Phys. Control. Fusion* 54 (2012) 085013
- [40] T. Schreiber Measuring Information Transfer Phys. Rev. Lett. 85 (2000) 461
- [41] B.Ph. van Milligen, J.H. Nicolau, B. Liu *et al* Filaments in the edge confinement region of TJ-II *Nucl. Fusion* 58 (2018) 026030